ELSEVIER

Biophysical Chemistry 134 (2008) 178–184

Biophysical Chemistry

http://www.elsevier.com/locate/biophyschem

Prediction of the binding modes between BB-83698 and peptide deformylase from *Bacillus stearothermophilus* by docking and molecular dynamics simulation

Qiang Wang [a], Jianwu Wang [b], Zhengting Cai [a,*], Weiren Xu [c]

[a] *Institute of Theoretical Chemistry, Shandong University, Jinan 250100, China*
[b] *Institute of Organic Chemistry, Shandong University, Jinan 250100, China*
[c] *Tianjin Institute of the Pharmaceutical Research, Tianjin 300193, China*

Received 15 December 2007; received in revised form 10 February 2008; accepted 11 February 2008
Available online 16 February 2008

Abstract

BB-83698 is a first potent inhibitor of peptide deformylase in this novel class to enter clinical trials. In this study, automated docking, molecular dynamics simulation and binding free energy calculations with the linear interaction energy (LIE) method are first applied to investigate the binding of BB-83698 to the peptide deformylase from *Bacillus stearothermophilus*. The lowest docking energy structure from each cluster is selected as different representative binding modes. Compared with the experimental data, the results show that the binding of BB-83698 in Mode **1** is the most stable, with a binding free energy of −41.35 kJ/mol. The average structure of the Mode **1** complex suggests that inhibitor interacts with Ile59 and Gly109 by hydrogen bond interaction and with Pro47, Pro57, Ile59 and Leu146 by hydrophobic interaction are essential for the activity of BB-83698. Mode **2** represents a new binding mode. Additionally, if the hydrophilic group is introduced to the benzo-[1,3]-dioxole ring, the binding affinity of BB-83698 to the peptide deformylase from *B. stearothermophilus* will be greatly improved.

Keywords: BB-83698; Peptide deformylase; *Bacillus stearothermophilus*; Docking; Molecular dynamics simulation

1. Introduction

In eubacteria, protein synthesis requires newly synthesized peptides to start with methionine, resulting in a formylated N-terminus in each nascent polypeptide [1]. The formyl moiety is removed by the sequential action of peptide deformylase (PDF) and a methionine amino peptidase in order to afford the mature protein [2–4].The gene encoding PDF (*def*) is essential for protein synthesis in a variety of pathogenic bacteria but is not required for mammalian protein synthesis [5,6], deformylation is therefore a crucial step in bacterial protein biosynthesis. The specific bacterial requirement for PDF in protein synthesis provides a rational basis for selectivity, making it an attractive potential drug discovery target [7–11].

The amino acid sequences show that PDF includes two different types: type I PDF and type II PDF [12]. In *Bacillus* sp., the type II PDF is the major PDF and the main target of the specific antibiotic actinonin [12,13]. Actinonin is a naturally occurring antibacterial agent [14] that is recently shown to be a potent PDF inhibitor exhibiting antibacterial activity against a wide range of different bacterial species [15]. The structure of PDF from *Bacillus stearothermophilus* (*B. stearothermophilus*) is reported to be of type II and the crystal structures of *B. stearothermophilus* PDF have also been solved and identified [12]. In the active site of this complex, the Ni atom is co-ordinated by two oxygen atoms of the hydroxamate group of actinonin, the carbonyl oxygen atom of Gln65, the Sγ atom of Cys110, and the imidazole N-ε2 atoms of His153 and His157. Hydrogen bonds are made between P1′ carbonyl and the main-

* Corresponding author. Tel.: +86 531 88365746; fax: +86 531 88564464.
E-mail address: zhtcai@sdu.edu.cn (Z. Cai).

0301-4622/$ - see front matter © 2008 Elsevier B.V. All rights reserved.
doi:10.1016/j.bpc.2008.02.003

chain NH of Ile59 and also between the main-chain carbonyl oxygen and NH groups of Gly109 and the P2′ NH and carbonyl groups, respectively. In the P2′ position, the isopropyl of ligand is exposed to solvent. More interactions between actinonin and protein are described in Ref. [12]. While early attempts to develop a series of hydroxamic acid analogues of actinonin never reached clinical development due to poor in vivo activity [16,17].

BB-83698 is a first potent inhibitor of PDF in this novel class to progress to clinical trials [18] and represents the potential new class of antibiotics for the treatment of community respiratory tract infections [19]. Its mechanism of action is through inhibition of the essential bacterial enzyme PDF [19]. BB-83698 has demonstrated antibacterial activity against *Streptococcus pneumoniae*, *Moraxella catarrhalis*, *Group A streptococci*, *Mycoplasma pneumoniae*, *Chlamydia pneumoniae and Legionella pneumophila* [20–23]. Although *B. stearothermophilus* PDF is a representative type II PDF [12], the structural information about the *B. stearothermophilus* PDF binding mode of BB-83698 is still unknown. So we perform a flexible molecular docking combined with a molecular dynamics (MD) simulation and binding free energy calculations to rationally predict the binding mode of BB-83698 and *B. stearothermophilus* PDF. The protein structure of *B. stearothermophilus* PDF is extracted from the crystal complex and the ligand structure is built on modifying inhibitor actinonin (1lqy) [12]. To consider the flexibility of protein, MD is further used based on docking results. Three conformations with lowest docking energy are selected for following MD analysis. The resulting average structures are compared with each other and also compared with the experimental data, which is expected to provide a reasonable binding mode of BB-83698 and *B. stearothermophilus* PDF.

2. Compounds and computational methodology

2.1. Models and docking

In the present study, the starting model for docking was built up based on the X-ray crystal structure at 1.90 Å resolution taken from the Protein Data Bank (pdb code, 1lqy) [12].

The Sybyl 7.0 package [24] was used to prepare the docking files. For the protein, no crystal structure water existed in the active site, so all water molecules were removed. Polar hydrogen atoms were added to the protein using the biopolymer module. Kollman charges were also loaded on the protein. The minimized structure of actinonin was built on modifying the inhibitor in 1lqy [12]. All hydrogen atoms were added to BB-83698 and charges required for calculation were assigned using the Gasteiger–Hückel formation. AutoDock3.0.5 [25] was used for all docking calculations. A grid spacing of 0.375 Å and $60\times60\times60$ number of points was created for protein. Since the Lamarckian genetic algorithm (LGA) was more efficient than others, it was applied to search the conformational and orientational space of the inhibitors while keeping the protein structures rigid. All amide bonds were considered as non-rotable. For all dockings, 50 independent runs with a maximum number of 2,000,000 energy evaluations, a mutation rate of 0.02 and a crossover rate of 0.8 were used.

2.2. Molecular dynamics (MD) and binding free energy calculations

The energy minimum conformations from each cluster were applied as the initial structures in the following 3000 ps molecular dynamics simulations using GROMACS 3.3 software package [26] with oplsaa force field [27] in a NVT environment. The three model complexes were separately embedded in a triclinic box containing about 8160 preequilibrated water molecules described by the Simple Point Charge water (SPC) model [28], and the distance between protein and the edge of the box was set 10 Å. We used a cutoff of 9 Å for van der Waals interactions and the Particle-mesh Ewald (PME) method [29] for long-range electrostatics interactions. Periodic boundary conditions were applied in all directions. One Na^+ ion was placed in the system to replace water molecule in random positions, thus making the whole system neutral. The LINCS parameters algorithm [30] was used to constrain the lengths of the bonds involving hydrogen atoms, and the time step was set 0.002 ps. The box was filled with SPC water molecules. To relax the configuration of the solvent and the local strain (due to generation of hydrogen positions), and to remove bad van der Waals contacts (particles that are too close) a steepest descent minimization of 1000 steps was adopted, followed by a 20 ps MD run to warm the optimized structures to a finite temperature of 300 K. The time step used in all calculations was 0.002 ps. Then a 3000 ps MD run was performed. When the MD simulations finished, all analyses were performed using facilities within the GROMACS package and the figures of the molecular structures were generated using PyMOL software [31].

The binding affinity is calculated using linear interaction energy (LIE) method [32,33] which can estimate the binding free energy of ligand in bound and free states. The interaction energies are divided into an electrostatic term and a van der Waals term as described in the following equation:

$$\Delta G_{\text{bind}} = \alpha\left(\langle V_{l-s}^{\text{vdw}}\rangle_{\text{p}} - \langle V_{l-s}^{\text{vdw}}\rangle_{\text{w}}\right) + \beta\left(\langle V_{l-s}^{\text{el}}\rangle_{\text{p}} - \langle V_{l-s}^{\text{el}}\rangle_{\text{w}}\right) + \gamma$$

where the term $\langle V_{l-s}\rangle$ represents the thermal averages calculated over the MD simulations of the electrostatic (el) and van der Waals (vdW) energies for the ligand atoms in the bound (p) state and in the free (w) state. The difference (Δ) between different potential is scaled by different coefficients [33]. For the non-polar interaction, the coefficient of it is set to $\alpha=0.18$ [34], while for the polar contribution, the scaling factor is set to $\beta=0.50$ [35]. Since we are mainly concerned with relative affinities, the constant parameter γ is not adjusted.

3. Results and discussion

3.1. Multi-conformation docking of BB-83698 complex

The three dominant clusters ranked with the lowest energy scores are selected and the ligand conformations in each cluster are shown in Fig. 1. We can see that the docking conformations appear in the same active site, while the P3′ side chain of ligand points to different region of protein. Concerning the docking

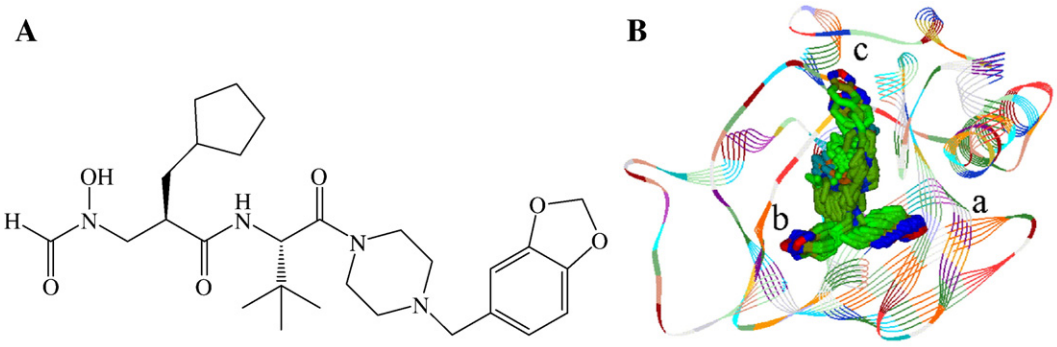

Fig. 1. (A) Structure of BB-83698. (B) The ligand conformations of the three clusters predicted by AutoDock. The protein is shown as a ribbon model and BB-83698 is shown as stick. The P3′ side chain of BB-83698 points to three different regions: a, b and c, respectively.

results, the docked energy in cluster 1 varies from −11.79 to −11.05 kcal/mol and the corresponding conformations of ligand appear in region **a**. The second and third clusters appear in region **b** and **c**, respectively, and their docked energies vary from −11.03 to −9.76 kcal/mol. This presents three different potential binding modes for BB-83698. Then the minimum energy conformation from each cluster is chosen as the best conformation for following MD simulation, which is named Mode **1**, Mode **2** and Mode **3**, respectively. In the Mode **1** complex, the P3′ side chain of BB-83698 is situated in the pocket which is composed of residues Gln45, Ile59, His76, Val77, Thr78 and Leu84. The benzo-[1,3]-dioxole oxygen interacts via H-bond with the amide hydrogen of Thr78, whereas the other one (O) bridges the amide group of Gln45. Besides the above mentioned residues, other residues (namely, Ile59, Leu61, Gln65, Glu108, Gly109, Cys110, Leu111, His153, Glu154 and His157) are in proper positions to be involved in electrostatic interactions with ligand. P1′ carbonyl group hydrogen bonds with the amide hydrogen of Ile59, moreover, P2′ amide hydrogen and carbonyl also form the hydrogen bonds with carbonyl and amide hydrogen of Gly109. The piperazine moiety at P3′ interacts with residues Ile59, Leu104, Thr106 and Leu146, which is likely responsible for the good ranking of this cluster.

Mode **2** represented in the second cluster is the closest one to Mode **1**. One obvious difference is that the P3′ side chain of ligand turns to the opposite region compared to Mode **1**. The P3′ side chain is surrounded by residues Leu104, Thr105, Thr106, Leu146, Ile182, Gly183 and Arg184, allowing the benzo-[1,3]-dioxole oxygen to form the hydrogen bonds with the amide hydrogens of Thr106 and Arg184. The piperazine ring approaches Ile59 and Leu146, which weakens the electrostatic interactions with Gly107 and Gly109.

Compared to Modes **1** and **2**, Mode **3** shows a distinct orientation. The *tert*-butyl is also exposed to solvent, but it makes the hydrophobic contact with Ile59 and Leu104. Similar to Mode **2**, the piperazine ring of ligand in Mode **3** is away from Gly109 and approaches Pro57 and Gly58. The benzo-[1,3]-bioxole group inserts a pocket which is composed of residues Ile7, Lys9, Tyr40, Arg56, Pro57, Cys110, Leu111, Val113 and Asp114, where it can hydrogen bond with the guanidinium group of Arg56. The lack of an H-bond interaction with Gly109 likely causes Mode **3** to be ranked at a higher docking energy score than Modes **1** and **2**, and the conformation of ligand seems unreasonable compared with that in the crystal complex of actinonin and *B. stearothermophilus* PDF. Finally, in order to check which mode is the most favorable and consider the flexibility of protein, we select above three modes for following MD simulations.

3.2. Protein root mean square deviation and flexibility

The 3000 ps MD simulations are successfully performed separately on the complexes of *B. stearothermophilus* PDF with the three modes. The physicochemical parameters such as potential reach stable value for all complexes after a few hundreds of picoseconds (see Fig. 2A).The root mean squared deviation (rmsd) fluctuations of backbone atoms compared with the initial structures are also obtained. Fig. 2B–D shows the rmsd of backbone atoms and ligands of the Mode **1**, Mode **2** and Mode **3** complexes as a function of time. After 1000 ps simulation, the three systems all reach equilibrium and the trajectories can be applied to collect snapshots for further analyses. By comparison with the three complexes, we can see that the Cα atoms have the similar rmsd, while those of ligands show obvious differences. The average rmsd of Cα atoms and ligand in the Mode **1** complex are 0.14 and 0.10 nm, those of the Mode **3** complex are 0.13 and 0.07 nm. During the MD simulations these two modes remain in a stable binding position with low rmsd fluctuations, confirming the feasibility of the binding poses predicted by AutoDock. We also observe that the rmsd of ligand in the Mode **2** complex increases rapidly to 0.24 nm at about 1000 ps and keeps fluctuating around this value until 3000 ps, which means that more large conformational changes have taken place for the Mode **2** complex.

3.3. Binding mode analysis

Fig. 3 shows the average structures of the three complexes using the trajectories after 1000 ps simulation. The orientations of the cyclopentyl ring from the three modes are identical and the cyclopentyl ring inserts the S1′ pocket which is composed of

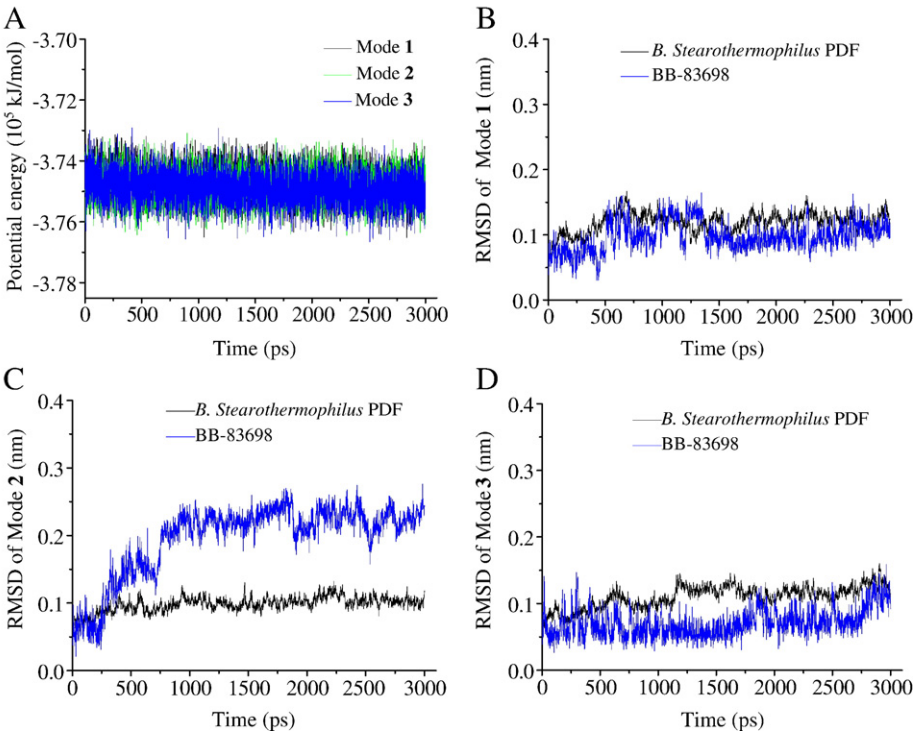

Fig. 2. (A) Potential energy evolution during the simulation time of three model complexes. (B, C and D) Root mean square derivation (nm) of backbone atoms of *B. Stearothermophilus* PDF (black line) and BB-83698 (blue line) in the Mode 1 (B), Mode 2 (C) and Mode 3 (D) complexes compared with the initial docking structure. (For interpretation of the references to colour in this figure legend, the reader is referred to the web version of this article.)

residues Ile59, Leu104, Glu108, Leu146, Ile149, Val150 and His153. In addition, another common feature among the three modes is that the *tert*-butyls are all exposed to solvent, which is identical with the initial docking conformation. There are significant differences between the MD average structure and the initial docking structure for Mode **2** (Fig. 3). On one hand, although the *tert*-butyl of ligand is exposed to solvent, hydrophobic contacts with the pyrrolidine ring of Pro57 and *tert*-butyl of Leu111 are found. On the other hand, the benzo-[1,3]-dioxole group adopts a reverse 180° turn conformation along the axis of molecular main chain and makes hydrophobic contacts with Ala50, two prolines Pro47 and Pro57, which leads to the disappearance of the original hydrogen bonds with Thr106 and Arg184. Although the P3′ side chain deviates greatly from both the original docking position predicted by AutoDock and the crystal positions of the complex (1lqy), most negative binding free energy (Table 1) indicates Mode **2** may be a new binding mode for the BB-83698/*B.stearothermophilus* PDF complex. Compared with Mode **2**, the conformational change of Mode **3** observed in our MD simulations also allows for a conserved pattern of interactions with the protein. In Mode **3**, the MD simulation of the binding orientation of ligand demonstrates the stability of this complex, with maintaining the original hydrogen bonds to the protein. In addition, the benzo-[1,3]-dioxole group hydrogen bonds with the amide hydrogens of Arg115 and Asp116. We see that although Mode **3** maintains the docking conformation basically, MD sampling still does not make Mode **3** revert to the crystal positions of the crystal structure (1lqy). Mode **3** also shows a low rmsd value of backbone atoms (0.1 nm), while more important hydrogen bond interactions which exist in Mode **1** are lost, which results in the number of hydrogen bond formed in Mode **3** is fewer than those in Mode **1**. The binding modes represented in Fig. 3A–B are the closet one to the binding mode of actinonin in the crystallographic complex with *B. stearothermophilus* PDF. A comparison of Mode **1** and crystal structure shows a series of common interactions between the ligand and the protein. With the structure of the Mode **1** complex, most hydrogen bonds between the ligand and protein are kept. For example, hydrogen bond is made between P1′ carbonyl oxygen and the amide hydrogen of Ile59. P2′ amide hydrogen and carbonyl oxygen also form the hydrogen bonds with the carbonyl oxygen and amide hydrogen of Gly109. Additionally, piperazine ring makes hydrophobic contacts with the pyrrolidine ring of Pro57 and isobutyl of Ile59. Our proposed mode points to several hydrophobic residues around benzo-[1,3]-dioxole group, such as Pro57, Ile59 and Leu146, being responsible for the binding of BB-83698 to *B. stearothermophilus* PDF. The profitable hydrogen bonds between ligand and residues such as Ile59 and Gly109 and hydrophobic interactions between piperazine ring and residues Pro57 and Ile59 could play an important role in defining the interaction pathway between the P3′ side chain and protein. We also see that the benzo-[1,3]-dioxole group approaches Gln45, which suggests us that the introduction of electron-donating substituent such as NH or NH2 or OH onto the benzo-[1,3]-dioxole ring will form the hydrogen bond with the carbonyl oxygen of Gln45. On the other hand, the introduction of electron-withdrawing substituent such as carbonyl

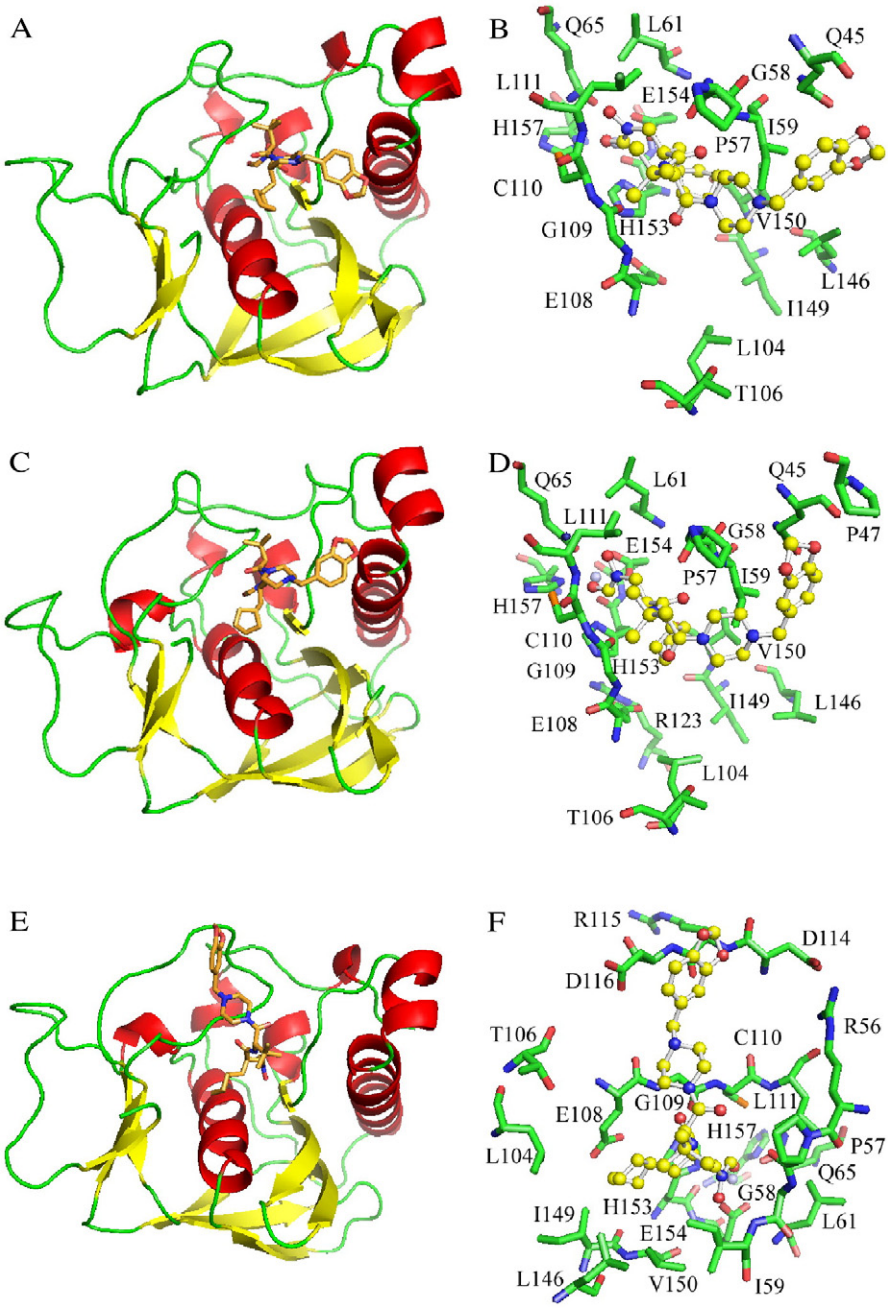

Fig. 3. Illustration to show the interactions between BB-83698 and *B. Stearothermophilus* PDF obtained by the MD simulations of the Mode 1 (A and B), Mode 2 (C and D) and Mode 3 (E and F) complexes. (A, C and E) an overview, ligand is shown with the stick representation and protein with cartoon drawing. (B, D and F) close view of the predicted (MD average) binding conformation. The residues are shown with the stick representation and ligand with ball-and-stick drawing.

onto the benzo-[1,3]-dioxole ring will also make the ligand interact with the amide hydrogen of Gln45 through hydrogen bond interactions, both of them will improve greatly the binding affinity of ligand to *B. stearothermophilus* PDF.

3.4. Binding free energy calculation

To find out the force for the ligand binding to *B. stearothermophilus* PDF, the electrostatic and van der Waals contributions to the interaction energies between the ligand and protein are calculated during the simulations, and the results are shown in Fig. 4. The binding free energy of Mode **2** is the most negative among the three modes, while an unexpected large deviation from the crystal positions of the complex indicates it may be a new binding mode. In addition, we put emphasis on Mode **1** and

Table 1
Comparison among calculated relative binding free energies (kJ/mol) and their components of three binding modes

Binding mode	Ligand-surrounding interactions				ΔG_{bind}
	$\langle V_{l-s}^{\text{el}}\rangle_{\text{w}}$	$\langle V_{l-s}^{\text{vdw}}\rangle_{\text{w}}$	$\langle V_{l-s}^{\text{el}}\rangle_{\text{p}}$	$\langle V_{l-s}^{\text{vdw}}\rangle_{\text{p}}$	
1	−202.29	−237.93	−162.43	−118.94	−41.35
2	−206.91	−238.34	−163.48	−119.16	−43.17
3	−186.40	−247.68	−164.96	−120.39	−33.63

compares it with Mode **3**. From Fig. 4 we see that the electrostatic interaction of the Mode **1** complex retains quite stable and its value keeps fluctuating around −149 kJ/mol during the simulations, indicating the initial hydrogen bonds between ligand and protein are maintained. The van der Waals energy of ligand with protein in the Mode **1** complex takes place from the start of the simulation, with the average of −175 kJ/mol. The van der Waals energy of the Mode **3** complex is comparable with that of the Mode **1** complex, while the lack of much hydrogen bond interactions existed in the Mode **1** complex probably causes a decreased affinity of ligand to the protein. The binding free energy of inhibitor is estimated with the linear interaction energy (LIE) method, the calculated electrostatic component of the binding free energy remains negative. Comparison of the ΔG values of the three model complexes reveals a large difference in their binding affinities. Table 1 shows that whether the electrostatic energies or van der Waals energies are in favor of the binding of ligand. The electrostatic interaction contributes −39.86 kJ/mol for the Mode **1** complex, while that for the Mode **3** complex is reduced to −21.44 kJ/mol. The electrostatic energy of the Mode **3** complex is smaller than that of the Mode **1** complex, indicating that electrostatic interaction favors Mode **1** more than Mode **3**. In all cases, a more large contribution from the hydrophobic component compared with electrostatic component of the binding free energy is observed. In the Mode **1** complex, the van der Waals contribution to the energies is −118.99 kJ/mol, about 79.13 kJ/mol more negative than electrostatic contribution (−39.86 kJ/mol). The estimated free energy of binding is therefore dominated by the hydrophobic contribution for Mode **1**. The binding free energy of Mode **1** is −41.35 kJ/mol, 7.72 kJ /mol more negative than Mode **3** (−33.63 kJ/mol). The results show that the reduced affinity of the Mode **3** complex is indeed mainly due to the marked reduction of hydrogen bonding (van der Waals contributions are comparable for the three model complexes). The more negative binding free energy and the reasonable interaction mode compared with experimental data show that Mode **1** is a preferable binding conformation for BB-83698.

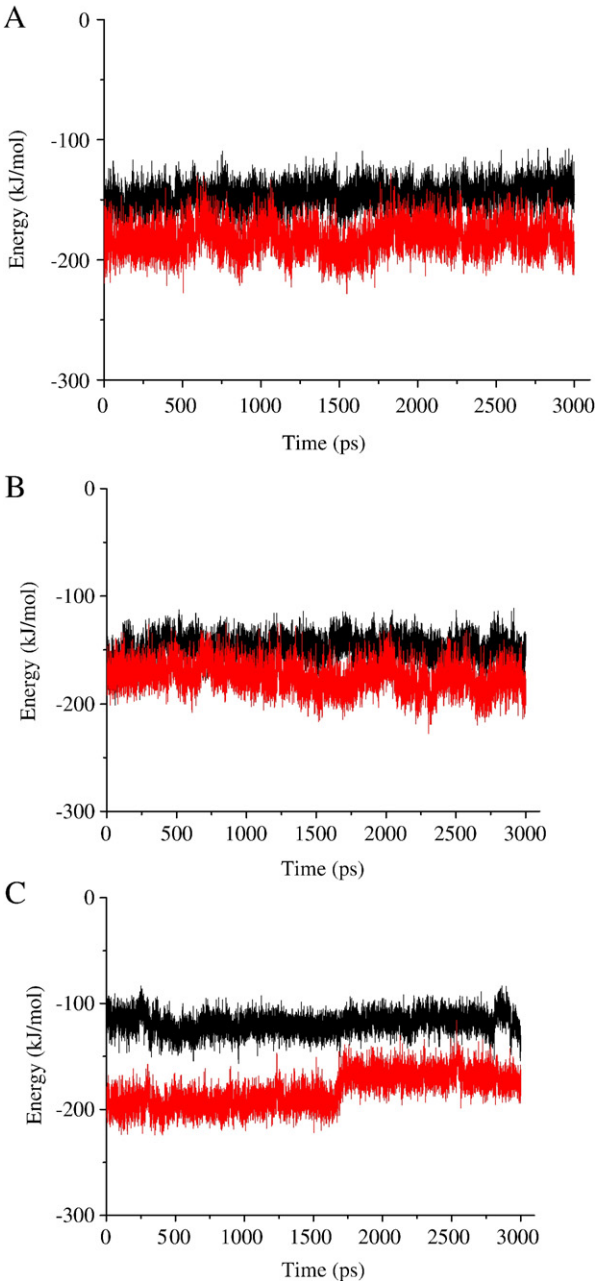

Fig. 4. Electrostatic (black) and Van der Waals (red) contributions to the energies of interaction between *B. Stearothermophilus* PDF and BB-83698 in the simulations of the Mode 1 (A), Mode 2 (B) and Mode 3 (C) complexes. (For interpretation of the references to colour in this figure legend, the reader is referred to the web version of this article.)

4. Conclusions

In this study, we try to identify the possible orientations of BB-83698 in the binding pocket of *B. stearothermophilus* PDF. The choice of binding modes of ligand is done by considering both the docking energy score and the binding affinities obtained by LIE method. Using the LIE method and the slightly modified model of actinonin inhibitor, we could predict the binding free energy differences of different modes of inhibitor bound to *B. stearothermophilus* PDF. After the simulation achieves the equilibrium, large conformational changes take place for Mode **2**, leading the ligand to deviate from both the original position predicted by AutoDock and the crystal positions of the complex greatly, while most negative binding free energy indicates it is a new binding modes which is different from that of crystal complex. At the same time, Mode **3** also does not revert to the positions of ligand in the crystal complex. The electrostatic interactions between ligand and protein in Mode **3** seem to be less tight than that of Mode **1**, because of a narrower interacting surface between the two moieties. These can explain why the binding affinity of Mode **1** is more negative than that of Mode **3**. In agreement with experimental data, the average structure of the Mode **1** complex based on the MD simulation suggests that the fundamental hydrogen bond interactions between the P1′ carbonyl and Ile59 amide and between the carbonyl and amide at the P2′ positions and Gly109 stabilize the binding of ligand and protein. In addition, the close interactions between piperazine ring and hydrophobic residue Pro57 and Ile59 and between the benzo-[1,3]-dioxole group and hydrophobic residue Pro57, Ile59 and Leu146 seem

to be particularly important for the binding of inhibitor to *B. stearothermophilus* PDF. All these allow for stronger interactions between ligand and protein, since the H-bond and hydrophobic interaction are more complete than that in docking conformation. We also notice that the introduction of hydrophilic group onto the benzo-[1,3]-dioxole ring will probably greatly increase the binding affinity of ligand to *B. stearothermophilus* PDF. The binding modes between BB-83698 and *B. stearothermophilus* PDF described here may be helpful for the design of new PDF inhibitors.

Acknowledgements

The authors acknowledge the supports of the National Key Basic Research Priority Program (2003CCA027) and the National Natural Science Foundation of China (Grant No. 20573064).

References

[1] T. Meinnel, Y. Mechulam, S. Blanquet, Methionine as translation start signal: a review of the enzymes of the pathway in *Escherichia coli*, Biochimie 75 (1993) 1061–1075.
[2] J.M. Adams, On the release of the formyl group from nascent protein, J. Mol. Biol. 33 (1968) 571–574.
[3] D.M. Livingston, P. Leder, Deformylation and protein biosynthesis, Biochemistry 8 (1969) 435–443.
[4] M. Takeda, R.E. Webster, Protein chain initiation and deformylation in *B. subtilis* homogenates, Proc. Natl. Acad. Sci. 60 (1968) 1487–1494.
[5] R. Wise, J.M. Andrews, J. Ashby, In vitro activities of peptide deformylase inhibitors against gram-positive pathogens, Antimicrob. Agents Chemother. 46 (2002) 1117–1118.
[6] P.M. Roblin, M.R. Hammerschlag, In vitro activity of a new antibiotic, NVP-PDF386 (VRC 4887), against *Chlamydia pneumoniae*, Antimicrob. Agents Chemother. 47 (2003) 1447–1448.
[7] C.M. Apfel, S. Evers, C. Hubschwerlen, W. Pirson, M.G.P. Page, W. Keck, Peptide deformylase as an Antibacterial drug target: assays for detection of its inhibition in *Escherichia coli* cell homogenates and intact cells, Antimicrob. Agents Chemother. 45 (2001) 1053–1057.
[8] C.M. Apfel, H. Locher, S. Evers, B. Takács, C. Hubschwerlen, W. Pirson, M.G.P. Page, W. Keck, Peptide deformylase as an antibacterial drug target: target validation and resistance development, Antimicrob. Agents Chemother. 45 (2001) 1058–1064.
[9] D. Pei, Peptide deformylase: a target for novel antibiotics? Emerg. Ther. Targets 5 (2001) 23–40.
[10] C.J. Hackbarth, D.Z. Chen, J.G. Lewis, Z. Yuan, et al., N-alkyl urea hydroxamic acids as a new class of peptide deformylase inhibitors with antibacterial activity, Antimicrob. Agents Chemother. 46 (2002) 2752–2764.
[11] D. Chen, C. Hackbarth, Z.J. Ni, C. Wu, Z. Yuan, et al., Peptide deformylase inhibitors as antibacterial agents: identification of VRC3375, a proline-3-alkylsuccinyl hydroxamate derivative, by using an integrated combinatorial and medicinal chemistry approach, Antimicrob. Agents Chemother. 48 (2004) 250–261.
[12] J.P. Guilloteau, M. Mathieu, C. Giglione, V. Mikol, et al., The crystal structures of four peptide deformylases bound to the antibiotic actinonin reveal two distinct types: a platform for the structure-based design of antibacterial agents, J. Mol. Biol. 320 (2002) 951–962.
[13] M. Haas, D. Beyer, R. Gahlmann, C. Freiberg, YkrB is the main peptide deformylase in *Bacillus subtilis*, a eubacterium containing two functional peptide deformylases, Microbiology 147 (2001) 1783–1791.
[14] J.J. Gordon, B.K. Kelly, G.A. Miller, Actinonin: an antibiotic substance produced by an actinomycete, Nature 18 (1962) 701–702.
[15] D.Z. Chen, D.V. Patel, C.J. Hackbarth, Z. Yuan, et al., Actinonin, a naturally occurring antibacterial agent, is a potent deformylase inhibitor, Biochemistry 39 (2000) 1256–1262.
[16] J.M. Clements, R.P. Beckett, A. Brown, et al., Antibiotic activity and characterization of BB-3497, a novel peptide deformylase inhibitor, Antimicrob. Agents Chemother. 45 (2001) 563–570.
[17] B.J. Broughton, P. Chaplen, W.A. Freeman, P.J. Warren, K.R.H. Wooldridge, D.E. Wright, Studies concerning the antibiotic actinonin. Part VIII. Structure-activity relationships in the actinonin series, J. Chem. Soc. Perkin Trans. 1 (1975) 857–860.
[18] D. Lofland, S. Difuntorum, A. Waller, J.M. Clements, M.K. Weaver, J.A. Karlowsky, K. Johnson, In vitro antibacterial activity of the peptide deformylase inhibitor BB-83698, J. Antimicrob. Chemother. 53 (2004) 664–668.
[19] E. Azoulay-Dupuis, J. Mohler, J.P. Bédos, Efficacy of BB-83698, a novel peptide deformylase inhibitor, in a mouse model of pneumococcal pneumonia, Antimicrob. Agents Chemother. 48 (2004) 80–85.
[20] S. Ramanathan-Girish, J. McColm, K.W. Johnson, et al., Pharmacokinetics in animals and humans of a first-in-class peptide deformylase inhibitor, Antimicrob. Agents Chemother. 48 (2004) 4835–4842.
[21] S.P. East, R.P. Beckett, D.C. Brookings, et al., Peptide deformylase inhibitors with activity against respiratory tract pathogens, Bioorg. Med. Chem. Lett. 14 (2004) 59–62.
[22] M. Gross, J. Clements, R.P. Beckett, W. Thomas, et al., Oral antipneumococcal activity and pharmacokinetic profiling of a novel peptide deformylase inhibitor, J. Antimicrob. Chemother. 53 (2004) 487–493.
[23] K.E. Bowker, A.R. Noel, A.P. MacGowan, In vitro activities of nine peptide deformylase inhibitors and five comparator agents against respiratory and skin pathogens, Int. J. Antimicro. Agents 22 (2003) 557–561.
[24] SYBYL modeling software, V7.0, Tripos Associates.
[25] G.M. Morris, D.S. Goodsell, R.S. Halliday, R. Huey, W.E. Hart, R.K. Belew, A.J. Olson, Automated docking using a Lamarckian genetic algorithm and an empirical binding free energy function, J. Comp. Chem. 19 (1998) 1639–1662.
[26] D. van der Spoel, E. Lindahl, B. Hess, G. Groenhof, A.E. Mark, H.J.C. Berendsen, Gromacs: fast, flexible, and free, J. Comp. Chem. 26 (2005) 1701–1718.
[27] W.L. Jorgensen, D.S. Maxwell, J. TiradoRives, Development and testing of the OPLS all-atom force field on conformational energetics and properties of organic liquids, J. Am. Chem. Soc. 118 (1996) 11225–11236.
[28] H.J.C. Berendsen, J.P.M. Postma, W.F. van Gunsteren, J. Hermans, Interaction models for water in relation to protein hydration, in: B. Pullman (Ed.), Intermolecular Forces, D. Reidel Publishing Company, Dordrecht, 1981, pp. 331–342.
[29] U. Essmann, L. Perera, M.L. Berkowitz, T. Darden, H. Lee, L.G. Pedersen, A smooth particle mesh Ewald method, J. Chem. Phys. 103 (1995) 8577–8593.
[30] B. Hess, H. Bekker, H.J.C. Berendsen, J.G.E.M. Fraalje, LINCS: a linear constraint solver for molecular simulations, J. Comp. Chem. 18 (1997) 1463–1472.
[31] W.L. DeLano, The PyMol Molecular Graphics System, DeLano Scientific, Palo Alto, CA, USA, 2002.
[32] J. Åqvist, C. Medina, J.E. Samuelsson, A new method for predicting binding affinity in computer-aided drug design, Protein Eng. 7 (1994) 385–391.
[33] T. Hansson, J. Marelius, J. Åqvist, Ligand binding affinity prediction by linear interaction energy methods, J. Comput. Aided Mol. Des. 12 (1998) 27–35.
[34] G. Götmar, T. Fornstedt, G. Guiochon, Apparent and true enantioselectivity in enantioseparations, Chirality 12 (2000) 558–564.
[35] F.S. Lee, Z.T. Chu, M.B. Bolger, A. Warshel, Calculations of antibody–antigen interactions: microscopic and semi-microscopic evaluation of the free energies of binding of phosphorylcholine analogs to McPC603, Prot. Eng. 5 (1992) 215–228.